(Preprint) AAS 23-350

INITIAL ORBIT DETERMINATION USING RELATIVE POSITION MEASUREMENTS

Sébastien Henry* **and John A. Christian** †

This work explores the problem of initial orbit determination (IOD) using relative position measurements between a pair of spacecraft in Keplerian orbits. We first show that the solution to this problem is not unique, even under certain classes of perturbations. We propose an algorithm to retrieve the inertial state of both orbiting spacecraft using the relative acceleration and Lambert's problem. Various options are compared to estimate the relative acceleration from a set of relative position measurements. Simulation results suggest that the proposed IOD algorithm is suitable for onboard navigation filter (re)initialization, and can thus improve constellation and formation-flying mission autonomy.

INTRODUCTION

Orbit determination has been investigated by mathematicians studying the movement of celestial bodies for centuries. Indeed, the discipline of orbit determination is tightly intertwined with the history of astrodynamics. For example, modern astrodynamics is built on the foundation laid by Kepler in the mid-1600s, when Kepler used observations from Tycho Brahe to deduce that the planets followed elliptical paths around the Sun.[1,2] The type problem solved by Kepler is what we refer to today as the initial orbit determination (IOD) problem—defined here as the task of estimating the orbit from a set of observations, but without any *a priori* knowledge of the orbit itself. We differentiate this from the companion problem of precise orbit determination (POD), which consists of using observations to refine the estimate of a known orbit, most commonly within a filter (either batch or sequential).

There exists a vast literature[3,4] on methods of IOD for a single orbiting object. The IOD task may be accomplished by direct observation of some of the spacecraft states, such as position (e.g., three position vectors and Gibbs problem[5]) or velocity (e.g., three velocity vectors and the orbital hodograph[6]). IOD for a single object may also be accomplished with measurements related to the state, such as a collection of line-of-sight measurements (i.e., angles-only methods[7–9]) or heading measurements.[10]

The modern era of spaceflight, however, continues to motivate new IOD problems that are different than those studied by classical mathematicians and astrodynamicists. For example, consider the case of two (or more) spacecraft in orbit wishing to mutually determine their orbits with only inter-satellite measurements.[11,12] Such an IOD scenario is of great practical relevance as we consider the problem of autonomous spacecraft constellations or formation flying missions. The two most

*Graduate Research Assistant, Guggenheim School of Aerospace Engineering, Georgia Institute of Technology, Atlanta, GA 30332.
†Associate Professor, Guggenheim School of Aerospace Engineering, Georgia Institute of Technology, Atlanta, GA 30332.

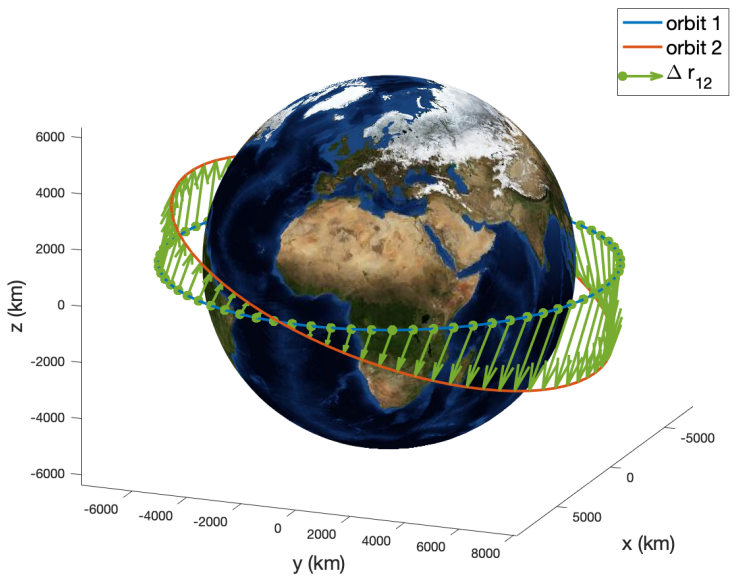

Figure 1: Strip formed by relative position measurements between two LEO satellites.

common types of inter-satellite measurements are range and bearing. The range may by obtained using the inter-satellite communication link,[13–16] radar,[17] or similar means. Two-satellite orbit determination using only inter-satellite range measurements (e.g., the LiAISON concept[18]) is possible for asymmetric orbits. Other sensors, such as cameras, provide the bearing from one spacecraft to another—which may often be expressed in the inertial frame using a background starfield. Combining concurrent range and bearing measurements provides a direct estimate of relative position. Several works have shown that the full state is observable with relative position measurements under most cases.[19–21]

Existing studies on the efficacy of inter-satellite position vectors for orbit determination use either batch filters[20] or sequential filters[19,21–26] to process a large number of measurements. All of these prior solutions depend on an initial guess of the orbit—and, thus, the prior literature focuses on the POD problem but *does not* address the IOD problem. To the authors' knowledge, there are no existing IOD methods to simultaneously determine the completely unknown Keplerian orbits of two satellites using only measurements of their relative position. In response to this gap, this paper develops a solution to the IOD problem using satellite relative position measurements. The IOD solution may then be provided to one of the existing POD solutions[19–26] for further refinement.

The remainder of this work develops as follows. In the first section, we show that the solution to this problem cannot be unique in Keplerian dynamics. Then, we propose a method for recovering the state and give practical considerations. Finally, we test the newly-proposed method on some generated examples.

PROBLEM DEFINITION

Consider two spacecraft orbiting a central gravitating body. Suppose that each of these spacecraft obeys Keplerian dynamics, with an orbital path described by a conic section. Let $\boldsymbol{r}_i$ be the inertial

position of the i-th spacecraft relative to the central body. Now, suppose this pair of spacecraft is capable of measuring the relative position vector between them at any point in time. Thus, each relative position measurement may be computed as

$$\Delta \boldsymbol{r}_{12}^k = \boldsymbol{r}_2^k - \boldsymbol{r}_1^k, \tag{1}$$

where the subscript k indicates the time t^k of the measurement. Over time a series of measurements $\{\Delta \boldsymbol{r}_{12}^k\}_{k=1}^n$ is formed as illustrated in Fig. 1 for two Low Earth Orbit (LEO) spacecraft. Define the state of the i-th object as its position (3×1 vector) and velocity (3×1 vector),

$$\boldsymbol{p}_i = \begin{bmatrix} \boldsymbol{r}_i \\ \dot{\boldsymbol{r}}_i \end{bmatrix}. \tag{2}$$

The purpose of the IOD is to determine the position and velocity of each object. Since this work treats the case where there are two objects, a total of 12 parameters need to be estimated ($\boldsymbol{p}_1$ and $\boldsymbol{p}_2$). The observability analyses conducted in Refs. [19,21,22] show that the initial states are locally observable, which is good enough for the POD (i.e., filtering) approaches used in these studies. In contrast to prior work, the IOD problem requires us to investigate the problem of global uniqueness of the solution. The following analysis shows that there will always be two different orbit pairs that produce a given time-history of relative position vectors, and so the IOD solution *cannot* be globally unique for Keplerian motion. Moreover, it is not globally unique under certain classes of orbital perturbations (e.g., J2 perturbations).

Theorem 1. *Let a pair of particles with states* $(\mathbf{p}_1, \mathbf{p}_2)$ *generate the sequence of relative position measurements* $\{\Delta \mathbf{r}_{12}^k\}_{k=1}^n$ *at times* $\{t^k\}_{k=1}^n$*. If the motion of both particles obey dynamics where the acceleration* $\mathbf{a}(\mathbf{p})$ *is an odd function* $\forall \mathbf{p}$*, then* $(-\mathbf{p}_2, -\mathbf{p}_1)$ *also generates the same sequence of measurements.*

Proof. We have a dynamical system with initial state

$$\boldsymbol{p}'(t^0) = \begin{bmatrix} -\boldsymbol{r}^0 \\ -\boldsymbol{v}^0 \end{bmatrix} = -\boldsymbol{p}(t^0). \tag{3}$$

The time derivative of the state is

$$\frac{d\boldsymbol{p}'(t)}{dt}\Big|_{t=t^0} = \begin{bmatrix} -\boldsymbol{v}^0 \\ \boldsymbol{a}(\boldsymbol{p}'(t^0)) \end{bmatrix} = -\begin{bmatrix} \boldsymbol{v}^0 \\ \boldsymbol{a}(\boldsymbol{p}(t^0)) \end{bmatrix} = -\frac{d\boldsymbol{p}(t)}{dt}, \forall t. \tag{4}$$

By virtue of the second fundamental theorem of calculus, the integrated state at the neighbouring time points will also be such that $\boldsymbol{p}'(t) = \boldsymbol{p}'(t)$ and the cycle continues. As time progresses, under an odd acceleration function,

$$\boldsymbol{p}'(t^0) = -\boldsymbol{p}(t^0) \Longleftrightarrow \boldsymbol{p}'(t) = -\boldsymbol{p}(t), \forall t. \tag{5}$$

It directly follows that

$$\begin{aligned} \Delta \boldsymbol{r}_{12}(t) &= \boldsymbol{r}_2(t) - \boldsymbol{r}_1(t) && \text{(6a)} \\ &= (-\boldsymbol{r}_1(t)) - (-\boldsymbol{r}_2(t)) && \text{(6b)} \\ &= \boldsymbol{r}_2'(t) - \boldsymbol{r}_1'(t) && \text{(6c)} \\ &= \Delta \boldsymbol{r}_{12}'(t), \ \forall t. && \text{(6d)} \end{aligned}$$

□

We note that acceleration from Newton's gravitational law is an odd function

$$\boldsymbol{a}_g(\boldsymbol{p}) = -\mu \frac{\boldsymbol{r}}{\|\boldsymbol{r}\|^3} = -\left(-\mu \frac{-\boldsymbol{r}}{\|\boldsymbol{r}\|^3}\right) = -\boldsymbol{a}_g(-\boldsymbol{p}). \tag{7}$$

Thus, by Theorem 1, the solution cannot be unique in Keplerian dynamics. Furthermore, it is not possible to use zonal harmonics of even degree (whose perturbation accelerations *are* odd functions, despite their name), or any sectoral harmonics to differentiate between the solutions. In particular, it is easy from Theorem 1 to prove that the acceleration from J_2 perturbation does *not* render the solution unique since[3,4]

$$\boldsymbol{a}_{J_2}(\boldsymbol{p}) = -\frac{3\mu J_2 R_{\text{body}}^2}{2\|\boldsymbol{r}\|^5} \begin{bmatrix} \left(1 - 5\left(\frac{z}{\|\boldsymbol{r}\|}\right)^2\right) x \\ \left(1 - 5\left(\frac{z}{\|\boldsymbol{r}\|}\right)^2\right) y \\ \left(3 - 5\left(\frac{z}{\|\boldsymbol{r}\|}\right)^2\right) z \end{bmatrix} = \frac{3\mu J_2 R_{\text{body}}^2}{2\|\boldsymbol{r}\|^5} \begin{bmatrix} \left(1 - 5\left(\frac{z}{\|\boldsymbol{r}\|}\right)^2\right) (-x) \\ \left(1 - 5\left(\frac{z}{\|\boldsymbol{r}\|}\right)^2\right) (-y) \\ \left(3 - 5\left(\frac{z}{\|\boldsymbol{r}\|}\right)^2\right) (-z) \end{bmatrix} = -\boldsymbol{a}_{J_2}(-\boldsymbol{p}). \tag{8}$$

Drag is also not a good candidate to separate the solutions if we use simple atmospheric models neglecting wind. Odd zonal harmonics (which don't have odd acceleration functions), such as J_3, and tesseral harmonics can help make the solution unique.

We can demonstrate this effect by taking the ISS example in Table 1. We reconstruct the initial states $\boldsymbol{p}_1^0$ and $\boldsymbol{p}_2^0$ and use a numerical integrator accounting for perturbations in J_2 to generate measurements every second, for a day. We also generate measurements in the alternative case where $\boldsymbol{p}_1^{0'} = -\boldsymbol{p}_2^0$ and $\boldsymbol{p}_2^{0'} = -\boldsymbol{p}_1^0$. We can observe on Fig. 2 that there is no discrepancy between the measurements generated by these two different initial conditions. By contrast, if we account for J_3 perturbation, then the measurements generated from the two initial conditions start to differ and it becomes possible to distinguish between them as seen in Fig. 3.

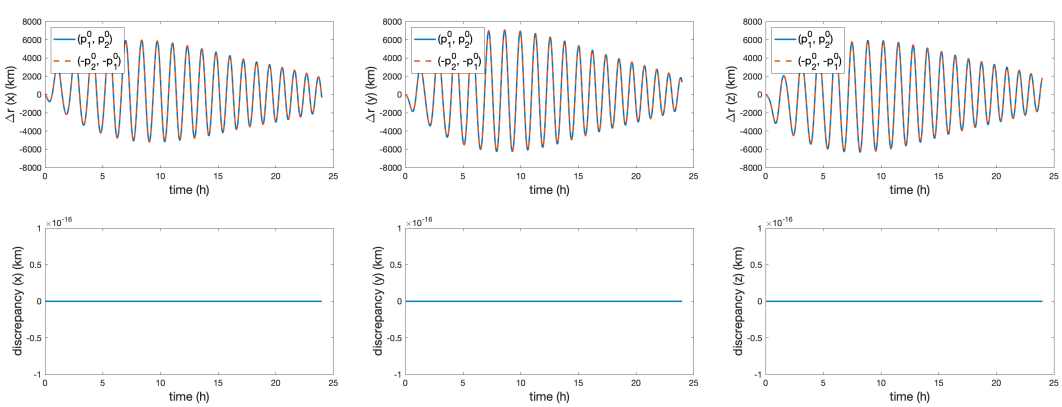

Figure 2: The relative measurements obtained propagating orbits with J_2 perturbation only are exactly the same with the two sets of initial conditions.

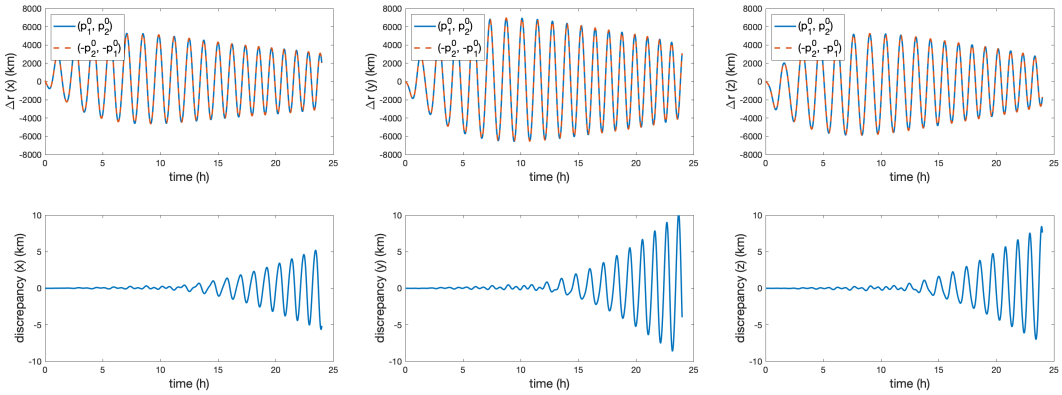

Figure 3: The relative measurements obtained propagating orbits with J_2 and J_3 perturbation differ depending on the two sets initial conditions.

IOD FROM RELATIVE POSITION VECTORS

As stated in the previous section, the purpose is to recover the position and velocity of the two objects, so 12 parameters in total. The complexity of a 12-dimensional search makes it difficult in practice to find a solution. We thus seek to reduce the dimensionality of that search. This can be achieved by considering the relative acceleration term. More detail about how to obtain an estimate for the relative acceleration is given later. Assuming Keplerian dynamics, we obtain the following expression

$$\Delta\ddot{\boldsymbol{r}}_{12} = -\mu\left(\frac{\boldsymbol{r}_2}{\|\boldsymbol{r}_2\|^3} - \frac{\boldsymbol{r}_1}{\|\boldsymbol{r}_1\|^3}\right). \tag{9}$$

Now, recognizing that $\boldsymbol{r}_2 = \boldsymbol{r}_1 + \Delta\boldsymbol{r}_{12}$, this becomes

$$\Delta\ddot{\boldsymbol{r}}_{12} + \mu\left(\frac{\boldsymbol{r}_1 + \Delta\boldsymbol{r}_{12}}{\|\boldsymbol{r}_1 + \Delta\boldsymbol{r}_{12}\|^3} - \frac{\boldsymbol{r}_1}{\|\boldsymbol{r}_1\|^3}\right) = \boldsymbol{0}_{3\times 1}. \tag{10}$$

Observe that Eq. (10) is a system of three nonlinear equations to solve concurrently, where $\boldsymbol{r}_1$ is the only unknown. Once solved, we directly find $\boldsymbol{r}_2 = \boldsymbol{r}_1 + \Delta\boldsymbol{r}_{12}$.

We solve the system at times t^i and t^j to obtain $\hat{\boldsymbol{r}}_1^i$ and $\hat{\boldsymbol{r}}_1^j$, and subsequently $\hat{\boldsymbol{r}}_2^i$ and $\hat{\boldsymbol{r}}_2^j$. Solving for two time stamps is enough to recover each orbit because we can then solve Lambert's problem twice *

$$[\hat{\boldsymbol{v}}_1^i, \hat{\boldsymbol{v}}_1^j] = \text{Lambert}(\hat{\boldsymbol{r}}_1^i,\, \hat{\boldsymbol{r}}_1^j,\, t^j - t^i), \tag{11a}$$

$$[\hat{\boldsymbol{v}}_2^i, \hat{\boldsymbol{v}}_2^j] = \text{Lambert}(\hat{\boldsymbol{r}}_2^i,\, \hat{\boldsymbol{r}}_2^j,\, t^j - t^i), \tag{11b}$$

where Eq. (11a) retrieves the full state (position and velocity) of object one, and Eq. (11b) retrieves the full state of object two.

In practice, we need to be more careful because the solution $\hat{\boldsymbol{r}}_1$ of Eq. (10) is not unique by virtue of Theorem 1. As a consequence, we have to consider Eq. (11a) with four pairs of position

*There are other options. For example, it may be possible to solve Eq. (10) at three-time stamps and use Gibbs methods,[5] but we do not explore this option here because it adds an extra time for which to solve.

inputs: $[\hat{\boldsymbol{r}}_1^i, \hat{\boldsymbol{r}}_1^j]$, $[-\hat{\boldsymbol{r}}_2^i, \hat{\boldsymbol{r}}_1^j]$, $[\hat{\boldsymbol{r}}_1^i, -\hat{\boldsymbol{r}}_2^j]$, and $[-\hat{\boldsymbol{r}}_2^i, -\hat{\boldsymbol{r}}_2^j]$. In the same respective order, Eq. (11b) has to be considered with $[\hat{\boldsymbol{r}}_2^i, \hat{\boldsymbol{r}}_2^j]$, $[-\hat{\boldsymbol{r}}_1^i, \hat{\boldsymbol{r}}_2^j]$, $[\hat{\boldsymbol{r}}_2^i, -\hat{\boldsymbol{r}}_1^j]$, and $[-\hat{\boldsymbol{r}}_1^i, -\hat{\boldsymbol{r}}_1^j]$. This gives us four candidate solutions. Two out of the four candidates can be removed by considering a relative position measurement at a third time. For that, we propagate the candidates to that time and prune the ones that are incoherent with the measurement. The two remaining candidates are indistinguishable in Keplerian dynamics because of Theorem 1. There is no choice but to use a more elaborate dynamical model or other types of measurements to isolate the truth.

Solutions to Lambert's problem being well established, the IOD problem has been reduced to estimating the acceleration and solving the nonlinear system in Eq. (10). To do this, we recognize that it can be further reduced to a planar problem and solved with standard optimization approaches. These two pieces will now be discussed in terms, and the estimation of the acceleration will be discussed in the following section.

Practical Considerations to Solve the System

While possible to solve the system at Eq. (10) directly, we prefer to multiply Eq. (10) by $\|\boldsymbol{r}_1\|^3$ to avoid the decrease as $\boldsymbol{r} \to \infty$ and get better numerical stability,

$$\|\boldsymbol{r}_1\|^3 \Delta\ddot{\boldsymbol{r}}_{12} + \mu \left(\|\boldsymbol{r}_1\|^3 \frac{\boldsymbol{r}_1 + \Delta\boldsymbol{r}_{12}}{\|\boldsymbol{r}_1 + \Delta\boldsymbol{r}_{12}\|^3} - \boldsymbol{r}_1 \right) = \boldsymbol{0}. \tag{12}$$

This operation adds a third solution to the equation at $\boldsymbol{r} = \boldsymbol{0}$, so we need to add a constraint that the norm of the position needs to be greater than the body radius. Denote the error as

$$\boldsymbol{\epsilon}(\boldsymbol{r}) = \|\boldsymbol{r}\|^3 \Delta\ddot{\boldsymbol{r}}_{12} + \mu \left(\|\boldsymbol{r}\|^3 \frac{\boldsymbol{r} + \Delta\boldsymbol{r}_{12}}{\|\boldsymbol{r} + \Delta\boldsymbol{r}_{12}\|^3} - \boldsymbol{r} \right). \tag{13}$$

We formulate the problem as a constrained minimization problem,

$$\hat{\boldsymbol{r}}_1 = \text{argmin}_{\boldsymbol{r}} \ \boldsymbol{\epsilon}(\boldsymbol{r})^T \boldsymbol{\epsilon}(\boldsymbol{r}), \tag{14a}$$

$$\text{such that} \quad \|\boldsymbol{r}\| - R_{body} > 0. \tag{14b}$$

In parallel, we observe that the problem has reduced from an incremental 12-dimensional search (two sets of position and velocity) down to two 3-dimensional searches ($\boldsymbol{r}_1^i$ and $\boldsymbol{r}_1^j$, solved independently). It can be further reduced to two 2-dimensional because the span of $\Delta\boldsymbol{r}_{12}$ and $\Delta\ddot{\boldsymbol{r}}_{12}$ forms a plane in which $\boldsymbol{r}_1$ and $\boldsymbol{r}_2$ must lie.

We may define the normal to the plane as

$$\hat{\boldsymbol{n}} = \frac{\Delta\ddot{\boldsymbol{r}}_{12} \times \Delta\boldsymbol{r}_{12}}{\|\Delta\ddot{\boldsymbol{r}}_{12} \times \Delta\boldsymbol{r}_{12}\|}, \tag{15}$$

The plane itself is spanned by two basis vectors that may be computed as

$$\hat{\boldsymbol{\ell}} = \frac{\Delta\boldsymbol{r}_{12}}{\|\Delta\boldsymbol{r}_{12}\|}, \tag{16}$$

$$\hat{\boldsymbol{m}} = \hat{\boldsymbol{\ell}} \times \hat{\boldsymbol{n}}. \tag{17}$$

These basis vectors form the rows of the rotation matrix that brings a vector from the original inertial frame into a new frame with bases $\{\hat{\boldsymbol{\ell}}, \hat{\boldsymbol{m}}, \hat{\boldsymbol{n}}\}$

$$\boldsymbol{T} = \begin{bmatrix} \hat{\boldsymbol{\ell}}^T \\ \hat{\boldsymbol{m}}^T \\ \hat{\boldsymbol{n}}^T \end{bmatrix}. \tag{18}$$

The relative position measurement and the relative acceleration are expressed in the set of plane coordinates as

$$\Delta \boldsymbol{r}_{12}^{\parallel} = \boldsymbol{T} \Delta \boldsymbol{r}_{12} \tag{19}$$

$$\Delta \ddot{\boldsymbol{r}}_{12}^{\parallel} = \boldsymbol{T} \Delta \ddot{\boldsymbol{r}}_{12}. \tag{20}$$

Solve Eq. (14) for $\boldsymbol{r}_1^{\parallel}[1:2]$ using vectors $\Delta \boldsymbol{r}_{12}^{\parallel}[1:2]$ and $\Delta \ddot{\boldsymbol{r}}_{12}^{\parallel}[1:2]$. The third component of any of those vectors is zero. Then retrieve the inertial position

$$\boldsymbol{r}_1 = \boldsymbol{T}^T \boldsymbol{r}_1^{\parallel}. \tag{21}$$

A representation of what the cost function in Eq. (14) looks like on the search plane is displayed in Fig. 4 for two LEO spacecraft. We observe two global minima which are the solutions for $\boldsymbol{r}$ corresponding to the position of spacecraft 1 and to the opposite position of spacecraft 2. These global minima are unconstrained because the flying spacecraft have nonzero altitudes. In addition, there are constrained local minima due to the artificial solution at the origin.

Multiple methods, whose convergence typically depends on an initial estimate, exist to solve this kind of constrained minimization problem.[27] But, because of the planar property, solving for r_1 is also practically feasible with a $n \times n$ grid search of complexity $\mathcal{O}(n^2)$. For better accuracy and speed, one may do a sequence of grid searches, starting with a course mesh and refining it around the minimum.

Observability

The full state observability of the system was first studied in the pioneering work of Markley.[19] Markley concluded that the full state would be unobservable in the case where two orbits have the same semi-major axis and eccentricity, and crossed their respective periapsis at the same time. In addition, the two orbits had to be coplanar or oriented so that they cross the line of intersection of the two planes at the same time. This statement has since then been generalized to the case of any orbit having the same semi-major axis, same eccentricity, and same eccentric anomaly, without the additional conditions.[21,22]

We observe that in that case $\|\boldsymbol{r}_1\| = \|\boldsymbol{r}_2\|$ at any time. In the case of $\|\boldsymbol{r}_1\| = \|\boldsymbol{r}_2\|$, we see from Eq. (9) that $\Delta \boldsymbol{r}_{12} \propto \Delta \ddot{\boldsymbol{r}}_{12}$. Consequently, the plane normal from Eq. (15) becomes $\hat{\boldsymbol{n}} \propto \Delta \boldsymbol{r}_{12} \times \Delta \ddot{\boldsymbol{r}}_{12} = \boldsymbol{0}_{3\times 1}$ and is ill-defined. We see from Eq. (12) that the solution for $\boldsymbol{r}_1$ cannot be collinear with $\Delta \boldsymbol{r}$ and $\Delta \ddot{\boldsymbol{r}}$ since this would only happen in two unrealistic cases:

1. $\boldsymbol{r}_1 = \boldsymbol{r}_2$, meaning that both objects occupy the same point in space at the same time
2. $\boldsymbol{r}_1 = -\boldsymbol{r}_2$, meaning that the objects are on geometrically opposite sides of the main body and have no possibility to create a measurement

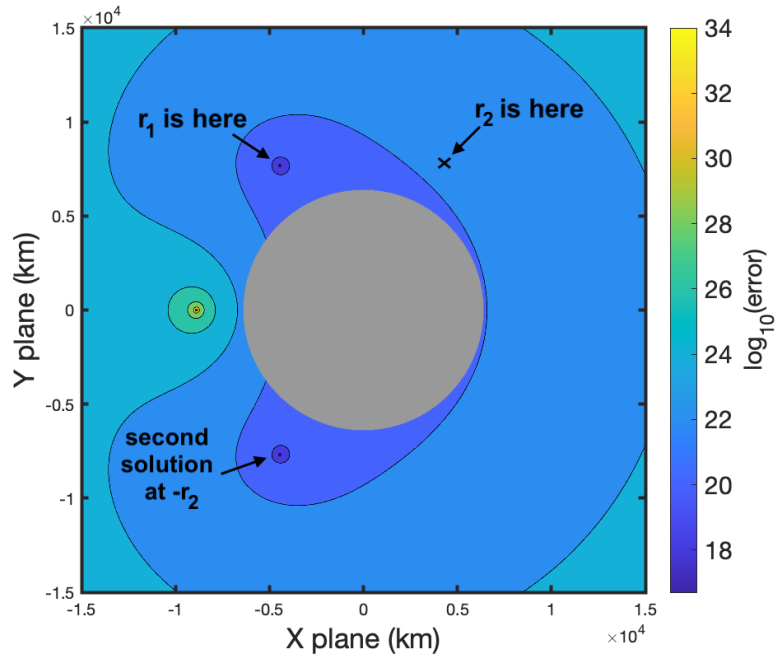

Figure 4: Square root of the cost function in Eq. (14) over the plane defined by $\Delta\boldsymbol{r}_{12}$ and $\Delta\ddot{\boldsymbol{r}}_{12}$ for two LEO spacecraft having the same orbit and phased by 60 deg in true anomaly.

There exists a solution to Eq. (12) on any plane that contains $\Delta\boldsymbol{r}$, but the solution is not collinear with $\Delta\boldsymbol{r}$. Since there are an infinite number of such planes, there are infinitely many solutions. This effect is demonstrated in the "rings of solutions" on Fig. 5, found by solving on a sequence of such planes.

CONSIDERATIONS FOR COMPUTING THE RELATIVE ACCELERATION

The developed IOD method requires knowledge of the relative acceleration to work. Because it is not directly available in the way this problem is set, we seek to estimate the relative acceleration $\Delta\ddot{\boldsymbol{r}}_{12}$ using the sequence of available measurements $\{\Delta\boldsymbol{r}_{12}^k\}_{k=1}^n$. It is well known that estimating derivatives is challenging on noisy data. Despite these difficulties, a great variety of effective methods exist. We illustratively explore a few of them in this work, including: finite differencing,[28] polynomial fits,[29] and finite impulse response (FIR) differentiators.[30] The effectiveness of each method greatly depends on the data available, i.e. the number of measurements and the time between them. With only three measurements, we can use the central difference scheme for a second derivative

$$\Delta\ddot{\boldsymbol{r}}_{12}^i \approx \frac{\Delta\boldsymbol{r}_{12}^{i+1} - 2\Delta\boldsymbol{r}_{12}^i + \Delta\boldsymbol{r}_{12}^{i-1}}{\Delta t^2}. \tag{22}$$

For given relative dynamics, a Δt that is too small poses stability problems on the finite difference, which are further amplified by noise. For that reason it is better to have a Δt that is moderately larger—it will not give a very accurate value of the relative acceleration but will be more robust to noise and more numerical stable. This effect is illustrated in Fig. 6 where IOD is on the lunar formation of Table 1. There are also central difference schemes that work with irregular time steps

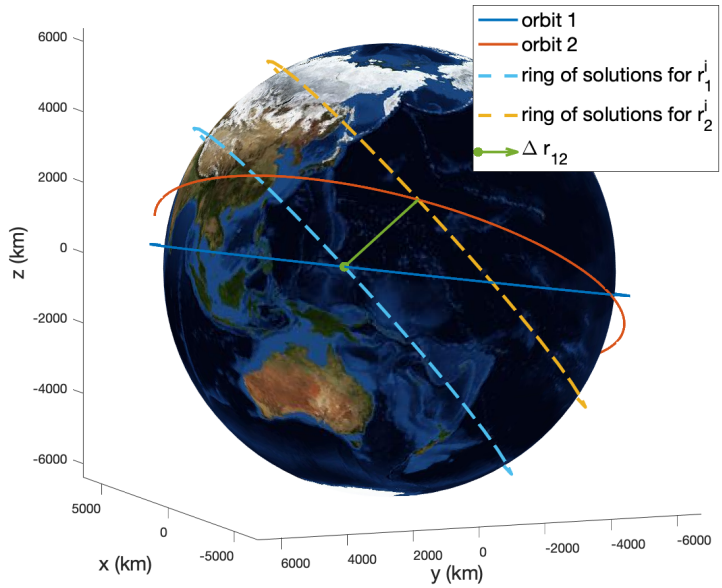

Figure 5: Rings of solutions to Eq. (12) in the case of two circular orbits with the same semi-major axis.

and can be extended to more than three measurements.[28,31] We also explore polynomial fits when more measurements are available. Polynomials are convenient because they are smooth functions that have simple analytical expressions for their second derivative. Alternatively, another popular method to differentiate a discrete signal is to analyze it in the frequency domain instead of the time domain. Given the power spectral density of the signal, one can design a finite impulse response (FIR) differentiation filter.[30] We apply the FIR differentiator twice to obtain the acceleration. The literature suggests it can work reasonably well when the order of the filter is sufficiently high, typically over $N = 100$.[32]

LINEAR COVARIANCE ANALYSIS

Along with an initial estimation of the state, a navigation filter will need to receive an initial covariance matrix before sequential refinements. This section highlights one way to estimate the covariance matrices of the states of both spacecraft of the IOD method presented in this paper. Start by noting that the relative inertial position measurement is typically obtained by the combination of a camera/bearing measurement and a range measurement. It is then possible to decompose the measurement as

$$\Delta\tilde{\boldsymbol{r}}_{12} = \tilde{\rho}\tilde{\boldsymbol{T}}_I^C \frac{\tilde{\boldsymbol{x}}}{\|\tilde{\boldsymbol{x}}\|} \tag{23}$$

where ρ is the range, $\boldsymbol{T}_I^C$ is rotation matrix from camera to inertial frame, and $\boldsymbol{x}$ is the measurement on the normalized image plane expressed in homogeneous coordinates.[33] The tilde overscript highlights that each term has been estimated with a noisy sensor. It is often assumed that the spacecraft attitude is perfectly known, but we model it here with for completeness. To a first order, the noisy rotation matrix as $\tilde{\boldsymbol{T}}_I^C = \boldsymbol{T}_I^C\,(\boldsymbol{I} - [\boldsymbol{\delta\phi}\times])$,[34] where $\boldsymbol{\delta\phi}$ is the rotation vector due to noise and

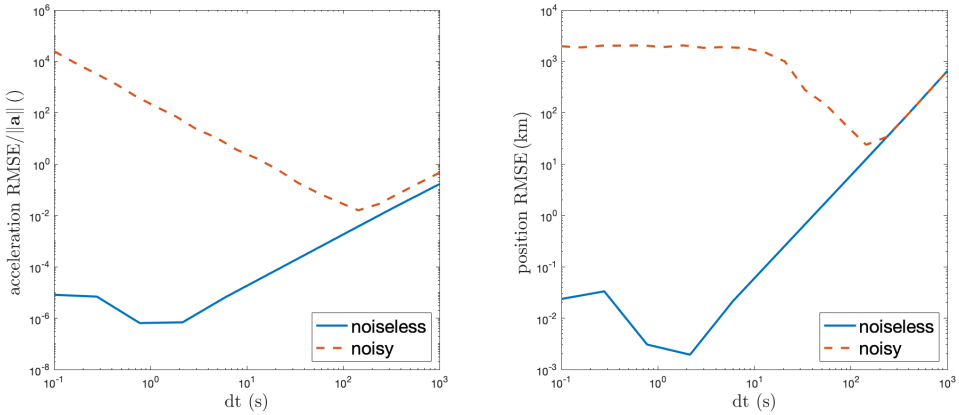

Figure 6: The quality of the IOD solution using finite difference depends on the time between the measurements, illustrated on the LLO case of Table 1.

$[\cdot\times]$ is the cross product matrix operator. Denote the sensitivity matrices of the relative position measurement with respect to the range, the attitude and the image plane measurement,

$$\boldsymbol{H}_\rho = \frac{\partial \Delta \boldsymbol{r}_{12}}{\partial \rho} = \boldsymbol{T}_I^C \frac{\boldsymbol{x}}{\|\boldsymbol{x}\|}, \tag{24a}$$

$$\boldsymbol{H}_{\delta\phi} = \frac{\partial \Delta \boldsymbol{r}_{12}}{\partial \delta\phi} = \rho \boldsymbol{T}_I^C \frac{[\boldsymbol{x}\times]}{\|\boldsymbol{x}\|}, \tag{24b}$$

$$\boldsymbol{H}_{\boldsymbol{x}} = \frac{\partial \Delta \boldsymbol{r}_{12}}{\partial \boldsymbol{x}} = \frac{\rho}{\|\boldsymbol{x}\|} \boldsymbol{T}_I^C \left(\boldsymbol{I} - \frac{\boldsymbol{x}\boldsymbol{x}^T}{\|\boldsymbol{x}\|^2} \right). \tag{24c}$$

These matrices allow us to write the covariance matrix of the relative position measurement

$$\boldsymbol{R}_{\Delta \boldsymbol{r}_{12}} = \sigma_\rho^2 \boldsymbol{H}_\rho \boldsymbol{H}_\rho^T + \boldsymbol{H}_{\delta\phi} \boldsymbol{R}_{\delta\phi} \boldsymbol{H}_{\delta\phi}^T + \boldsymbol{H}_{\boldsymbol{x}} \boldsymbol{R}_{\boldsymbol{x}} \boldsymbol{H}_{\boldsymbol{x}}^T. \tag{25}$$

The covariance of the relative acceleration will depend on the method used to approximate it. In the case of central difference, we can use uncertainty propagation assuming independent measurements to get

$$\boldsymbol{R}_{\Delta \ddot{\boldsymbol{r}}^i} = \frac{\boldsymbol{R}_{\Delta \boldsymbol{r}_{12}^{i+1}} + 4\boldsymbol{R}_{\Delta \boldsymbol{r}_{12}^{i}} + \boldsymbol{R}_{\Delta \boldsymbol{r}_{12}^{i-1}}}{\Delta t^4}. \tag{26}$$

We cannot in general consider identically distributed measurements because the range measurement, attitude of the spacecraft, and image plane measurement may change through time. Equation (26) highlights the main problem of central difference on noisy data as the variance of the process increases as Δt decreases, but the bias increases in $\mathcal{O}(\Delta t^2)$. Hence a compromise needs to be found for the time step of noisy finite difference.

Now that the covariance matrices of the relative position and acceleration have been found, we can proceed to the estimation of the position covariance. Given that there is no closed form solution to Eq. (14), we can evaluate the uncertainty propagation using finite difference or an unscented transform. If finite difference is used, then we obtain numerical values for $\frac{\partial \boldsymbol{r}}{\partial \Delta \boldsymbol{r}_{12}}$ and $\frac{\partial \boldsymbol{r}}{\partial \Delta \ddot{\boldsymbol{r}}_{12}}$ and

express

$$\boldsymbol{R}_{\boldsymbol{r}_1} = \frac{\partial \boldsymbol{r}_1}{\partial \Delta \boldsymbol{r}_{12}} \boldsymbol{R}_{\Delta \boldsymbol{r}_{12}} \frac{\partial \boldsymbol{r}_1}{\partial \Delta \boldsymbol{r}_{12}}^T + \frac{\partial \boldsymbol{r}_1}{\partial \Delta \ddot{\boldsymbol{r}}_{12}} \boldsymbol{R}_{\Delta \ddot{\boldsymbol{r}}_{12}} \frac{\partial \boldsymbol{r}_1}{\partial \Delta \ddot{\boldsymbol{r}}_{12}}^T, \tag{27a}$$

$$\boldsymbol{R}_{\boldsymbol{r}_2} = \frac{\partial \boldsymbol{r}_2}{\partial \Delta \boldsymbol{r}_{12}} \boldsymbol{R}_{\Delta \boldsymbol{r}_{12}} \frac{\partial \boldsymbol{r}_2}{\partial \Delta \boldsymbol{r}_{12}}^T + \frac{\partial \boldsymbol{r}_2}{\partial \Delta \ddot{\boldsymbol{r}}_{12}} \boldsymbol{R}_{\Delta \ddot{\boldsymbol{r}}_{12}} \frac{\partial \boldsymbol{r}_2}{\partial \Delta \ddot{\boldsymbol{r}}_{12}}^T. \tag{27b}$$

The position covariance matrices need to be computed for both spacecraft at the starting time t^i and the final time t^j.

Finally, we want to quantify the uncertainty in velocity which is obtained through Lambert's problem. Once the Lambert problem is solved, one can obtain the sensitivity matrices between the differences in states at t^i and t^j,

$$\begin{pmatrix} \delta \boldsymbol{r}^j \\ \delta \boldsymbol{v}^j \end{pmatrix} = \begin{pmatrix} \boldsymbol{\Phi}_{rr} & \boldsymbol{\Phi}_{rv} \\ \boldsymbol{\Phi}_{vr} & \boldsymbol{\Phi}_{vv} \end{pmatrix} \begin{pmatrix} \delta \boldsymbol{r}^i \\ \delta \boldsymbol{v}^i \end{pmatrix} \tag{28}$$

Following the same approach as proposed in Ref. 35, we propagate the position covariance through Lambert's problem using the sensitivity matrices in Eq. (28). It is possible to write the initial state $\boldsymbol{p}^i$ and final state $\boldsymbol{p}^j$ as a function of the initial and final positions,[35]

$$\boldsymbol{p}^i = \begin{pmatrix} \boldsymbol{r}^i \\ \boldsymbol{v}^i \end{pmatrix} = \underbrace{\begin{pmatrix} \boldsymbol{I} & \boldsymbol{0} \\ -\boldsymbol{\Phi}_{rv}^{-1}\boldsymbol{\Phi}_{rr} & \boldsymbol{\Phi}_{rv}^{-1} \end{pmatrix}}_{\boldsymbol{M}} \begin{pmatrix} \boldsymbol{r}^i \\ \boldsymbol{r}^j \end{pmatrix}, \tag{29}$$

$$\boldsymbol{p}^j = \begin{pmatrix} \boldsymbol{r}^j \\ \boldsymbol{v}^j \end{pmatrix} = \underbrace{\begin{pmatrix} \boldsymbol{0} & \boldsymbol{I} \\ \boldsymbol{\Phi}_{vr} - \boldsymbol{\Phi}_{vv}\boldsymbol{\Phi}_{rv}^{-1}\boldsymbol{\Phi}_{rr} & \boldsymbol{\Phi}_{vv}\boldsymbol{\Phi}_{rv}^{-1} \end{pmatrix}}_{\boldsymbol{N}} \begin{pmatrix} \boldsymbol{r}^i \\ \boldsymbol{r}^j \end{pmatrix}. \tag{30}$$

Denote the covariance matrix of the positions at both times

$$\boldsymbol{R}_r = \begin{pmatrix} \boldsymbol{R}_{\boldsymbol{r}^i} & \boldsymbol{0} \\ \boldsymbol{0} & \boldsymbol{R}_{\boldsymbol{r}^j} \end{pmatrix}, \tag{31}$$

where it is assumed that positions at different times are uncorrelated. The covariance of the state at t^i and at t^j are respectively

$$\boldsymbol{R}_{\boldsymbol{p}^i} = \begin{pmatrix} \boldsymbol{R}_{\boldsymbol{r}^i} & \boldsymbol{R}_{\boldsymbol{r}^i,\boldsymbol{v}^i} \\ \boldsymbol{R}_{\boldsymbol{r}^i,\boldsymbol{v}^i} & \boldsymbol{R}_{\boldsymbol{v}^i} \end{pmatrix} = \boldsymbol{M}\boldsymbol{R}_r\boldsymbol{M}^T, \tag{32}$$

$$\boldsymbol{R}_{\boldsymbol{p}^j} = \begin{pmatrix} \boldsymbol{R}_{\boldsymbol{r}^j} & \boldsymbol{R}_{\boldsymbol{r}^j,\boldsymbol{v}^j} \\ \boldsymbol{R}_{\boldsymbol{r}^j,\boldsymbol{v}^j} & \boldsymbol{R}_{\boldsymbol{v}^j} \end{pmatrix} = \boldsymbol{N}\boldsymbol{R}_r\boldsymbol{N}^T. \tag{33}$$

Equations (28) to (33) thus allow to compute the full state covariance of spacecraft 1 (starting from Eq. (27a)) or spacecraft 2 (starting from Eq. (27b)).

SIMULATION

We analyze the IOD algorithm performance on a variety of simulated spacecraft pairs, as shown in Table 1 and Fig. 7. The first pair is composed of two circular orbits with the same semi-major axis around Earth. We then analyze the case of a radio-astronomy formation with two nearly circular orbits of the same semi-major axis in low lunar orbit (LLO). The third pair takes the case of the ISS and an elliptic object also in low earth orbit (LEO). The orbit of the ISS was extracted from a two-line element on CelesTrak*. Finally, the last setup considers the case of a fly-by of Mars, where

*https://celestrak.org/

one spacecraft is on a hyperbolic fly-by and the other is in a slightly eccentric Mars orbit.

Table 1: Initial orbital elements of the pair of orbit tested.

Simulation	body	a (km)	e	i (deg)	Ω (deg)	ω (deg)	ν (deg)
Circular A	Earth	6797	0	10	30	10	10
Circular B		6797	0	30	40	20	5
LLO A	Moon	1938	0.005	27	30	10	0
LLO B		1938	0.007	27.2	30	10	0
ISS A	Earth	6797	0.00060	51.64	61.64	101.86	68.56
ISS B		7047	0.1006	56.64	61.64	101.86	68.50
Hyperbolic A	Mars	-16378	1.5	32	40	10	0
Eccentric B		7378	0.1	52	50	20	0

All of the orbits in Table 1 are given at $t = 0$. Each orbit is propagated using Keplerian dynamics (without any perturbation) and a series of inter-satellite position measurements is generated. Perfect measurements as well as noisy measurements are considered. In the noisy case, the range has a standard deviation of 10 cm and the direction has a standard deviation of 5 arcsec.

A series of refining grid searches is implemented to find the solution to Eq. (14). This option is chosen because it deals the most simply with the constraint. For all cases, we solve Eq. (14) at $t^i = 1000$s and $t^j = 2000$s and use the results to perform the Lambert problem. The Lambert problem is solved with the universal variable to accommodate all types of conics.[36] We then use a measurement at $t^k = 3000$s to eliminate two out of the four candidate solutions. The timeline is graphically shown in Fig. 8. It is assumed that a discriminating factor exists to remove the last candidate that will generate exactly the same set of measurements. Estimation is done fifty times for each pair to obtain the statistics.

We compare multiple methods to obtain $\Delta\ddot{\boldsymbol{r}}_{12}$. The exact value of the acceleration is known in the first one. The second method is the second-order central difference on the measurements using Eq. (22). An implementation of a more robust central difference scheme using more measurements is also considered.[31] A polynomial is fitted on the data and its second derivative is taken. For this method, we collect measurements for five minutes and try two different sample rates. The polynomial fit is of degree three when the sample rate is 10s, but its degree is increased to degree five when the sample rate is 1s. Finally, a FIR differentiator filter using MATLAB's builtin function is compared to the polynomial fit. The filter is of order 150 and has a pass band frequency of 10^{-4}Hz and a stop band frequency of 10^{-2}Hz. In our analysis, other parameters for the filters have shown much better performance in the noiseless case, but ended up with poor performance when noise was added. A summary of the different methods is proposed in Table 2, as well as a graphical representation of the arcs on Fig. 8.

We note that in a perfect world, it may be possible to use only 4 measurements to solve the entire IOD problem. For example use measurements 1, 2, and 3 to estimate acceleration at time 2 using central difference. Use measurements 2, 3, and 4 to estimate acceleration at time 3 using central difference. Use measurement 4 to discriminate. This will not work as well in practice because of the short time in the Lambert solver. The measurement arc set-ups summarized in Table 2 better reflect the type of data one might usually see in practice.

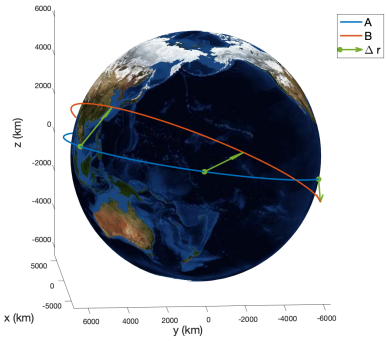

(a) Two circular orbits.

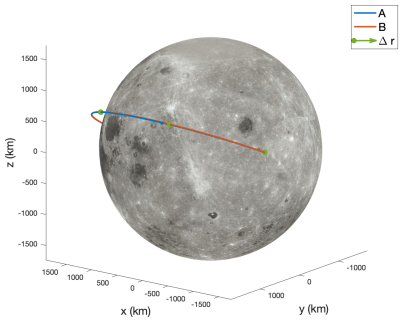

(b) LLO formation.

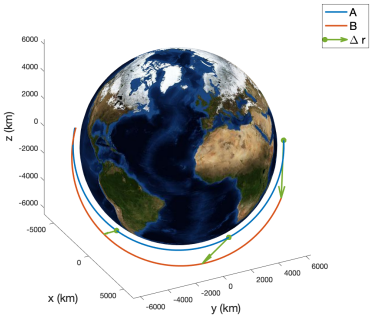

(c) ISS and elliptic object.

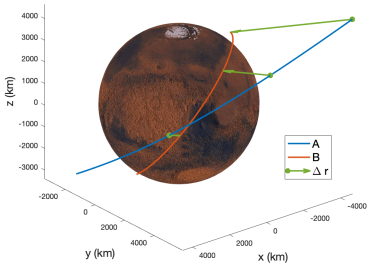

(d) Mars fly-by.

Figure 7: The four formations considered span a wide range of eccentricity.

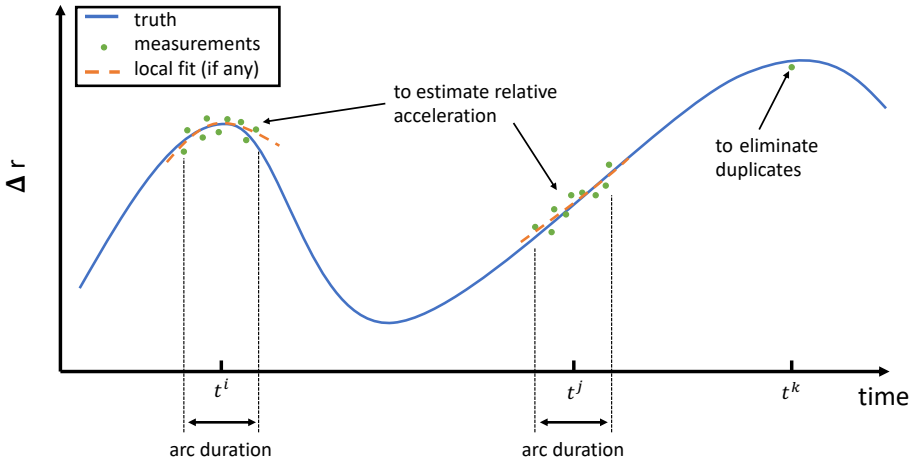

Figure 8: Illustration of the simulation setup.

Table 2: Summary of tested methods to find acceleration at a specific time. Measurements, when more than one, are evenly spread around the time of interest.

Method	number of $\Delta \boldsymbol{r}$ observations per arc	number of $\Delta \ddot{\boldsymbol{r}}$ observations per arc	arc duration (s)
Exact	1	1	N/A
CD	3	0	200
RCD	7	0	300
Poly-3	31	0	300
Poly-5	301	0	300
FIR	301	0	300

Results

The IOD estimates of position and velocity are each analyzed using three metrics: bias, standard deviation (σ), and root mean squared error (RMSE). We only display the performance metrics for the first spacecraft (spacecraft A), but note that the statistics were always of the same order for the other spacecraft (spacecraft B). The statistics are derived using a Monte-Carlo simulation of 50 samples and represent the state at final time of the Lambert problem.

The case of two circular orbits does not offer an accurate solution even in the case of exact acceleration and measurements, as shown in Table 3. If the eccentricity of both objects is changed to 10^{-6}, then the RMSEs of the position and velocity plummet to 10^{-7}km and 10^{-9} km/s, respectively. This stark difference confirms a singularity in this particular case. The case of two non-coplanar circular orbits with same semi-major axis had not been deemed unobservable in early studies,[19] but has since then been proven so by Psiaki[22] and by Li & Zhang.[21]

Table 3: Algorithm performance on the bi-circular pair with same semi-major axis, without noise.

Method	position bias (km)	position σ (km)	position RMSE (km)	velocity bias (m/s)	velocity σ (m/s)	velocity RMSE (m/s)
Exact	-	-	7.14×10^1	-	-	2.13×10^2

The result for the other formations are displayed in Tables 4 to 6. Using exact values for the acceleration yields position errors close to machine precision (because the position is itself in the thousands of km). The velocity errors are not quite at machine precision due to the tolerance on the Lambert solver. We note that the noise does no apparent effect on the solution when the perfect acceleration is known, so the degradation in performance is mainly due to the estimate of the acceleration.

For the methods approximating the acceleration, the RMSE of the estimated position with noise is in the 10's of km for the methods using few measurements, and under 10km for methods using many measurements. Similarly, velocity estimates have an RMSE of 10's of m/s for the methods using few measurements and under 10 m/s (except in the hyperbolic case) for methods using many measurements.

The simple central difference consistently makes the poorest approximation among the tested

Table 4: Algorithm performance on the LLO formation.

	Method	position bias (km)	position σ (km)	position RMSE (km)	velocity bias (m/s)	velocity σ (m/s)	velocity RMSE (m/s)
no noise	Exact	-	-	2.41×10^{-11}	-	-	1.89×10^{-7}
	CD	-	-	5.99	-	-	7.66
	RCD	-	-	1.05×10^{1}	-	-	1.34×10^{1}
	Poly-3	-	-	1.23×10^{1}	-	-	1.57×10^{1}
	Poly-5	-	-	1.78×10^{-2}	-	-	2.09×10^{-2}
	FIR	-	-	7.76	-	-	1.01×10^{1}
noise	Exact	2.41×10^{-11}	4.77×10^{-13}	2.41×10^{-11}	1.89×10^{-7}	7.93×10^{-14}	1.89×10^{-7}
	CD	7.94	4.41×10^{1}	4.44×10^{1}	7.84	3.98×10^{1}	4.02×10^{1}
	RCD	9.16	1.92×10^{1}	2.11×10^{1}	1.09×10^{1}	1.78×10^{1}	2.08×10^{1}
	Poly-3	1.19×10^{1}	7.41	1.40×10^{1}	1.55×10^{1}	6.91	1.70×10^{1}
	Poly-5	3.89×10^{-1}	8.28	8.21	1.82×10^{-1}	7.95	7.88
	FIR	7.20	4.18	8.31	9.79	3.80	1.05×10^{1}

methods in the case where there is noise, but still keeps an RMSE of under 50km in all scenarios. Even though the robust central difference has a higher bias than the regular central difference, it maintains a lower variance and in general a lower RMSE on noisy data. The proposed polynomial fits both work better than the central difference schemes. We note that the third-order polynomial keeps a very similar RMSE when noise is added, indicating better robustness to noise. Poly-5's performance worsens in the case of noise. Regardless, it still consistently exhibits the lowest position bias, variance, and RMSE on all scenarios with and without noise. The FIR filter approaches the RMSE performance of the Poly-5 method, but because of a high bias rather than a high variance. Its performance with and without noise are practically the same. Overall, all the methods performing with high bias in the noiseless case managed to keep a stable performance in the noisy simulation. This behavior is analogous to the so-called *bias-variance trade-off* of statistical models.[29]

Finally, we show the estimated value of the full state covariance of the LLO simulation. Table 7 shows the state covariance of spacecraft 1 obtained analytically with perfect measurements. Table 8 shows the state covariance of spacecraft 1 obtained with Monte-Carlo simulation of 100,000 samples. We observe a good agreement between those, with values in the same orders of magnitude in all the terms.

The philosophy behind IOD is to provide a sufficiently good first estimate to the POD algorithm for it to converge better and faster. Several POD filters[21,23,26] have been successfully tested with initial uncertainties in the same orders of magnitude as what our algorithm finds in the noisy case, even with central difference. This highlights the fact that our algorithm can provide good initial conditions for POD.

CONCLUSION

This work successfully introduces an algorithm to solve the IOD problem of two spacecraft using only inertial relative position measurements in the two-body problem. It shows that a symmetric geometry can generate the same measurement history, and thus the solution is not unique. Perturbations with odd acceleration functions cannot help to differentiate the two solutions. Assuming a discriminating factor exists, the algorithm retrieves the state to machine precision when given the exact relative acceleration. In a more challenging case where acceleration is estimated on noisy data,

Table 5: Algorithm performance on the ISS-LEO pair.

	Method	position bias (km)	position σ (km)	position RMSE (km)	velocity bias (m/s)	velocity σ (m/s)	velocity RMSE (m/s)
no noise	Exact	-	-	1.58×10^{-12}	-	-	9.66×10^{-7}
	CD	-	-	4.57	-	-	4.72
	RCD	-	-	8.00	-	-	8.28
	Poly-3	-	-	9.38	-	-	9.70
	Poly-5	-	-	9.53×10^{-3}	-	-	1.90×10^{-2}
	FIR	-	-	7.20	-	-	3.62
noise	Exact	1.58×10^{-12}	9.47×10^{-13}	1.58×10^{-12}	9.66×10^{-7}	2.02×10^{-12}	9.66×10^{-7}
	CD	4.01	2.69×10^{1}	2.69×10^{1}	6.42	2.57×10^{1}	2.62×10^{1}
	RCD	7.90	1.48×10^{1}	1.66×10^{1}	8.40	1.33×10^{1}	1.57×10^{1}
	Poly-3	9.12	4.86	1.03×10^{1}	1.01×10^{1}	5.00	1.13×10^{1}
	Poly-5	2.60×10^{-1}	6.27	6.21	4.16×10^{-1}	5.81	5.76
	FIR	7.27	2.95	7.84	3.72	2.71	4.59

Table 6: Algorithm performance on the Mars hyperbolic-elliptic pair.

	Method	position bias (km)	position σ (km)	position RMSE (km)	velocity bias (m/s)	velocity σ (m/s)	velocity RMSE (m/s)
no noise	Exact	-	-	4.28×10^{-12}	-	-	5.24×10^{-5}
	CD	-	-	4.02	-	-	4.47×10^{1}
	RCD	-	-	7.04	-	-	7.55×10^{1}
	Poly-3	-	-	8.25	-	-	8.75×10^{1}
	Poly-5	-	-	1.74×10^{-2}	-	-	1.26
	FIR	-	-	5.85	-	-	5.64×10^{1}
noise	Exact	4.28×10^{-12}	9.26×10^{-13}	4.28×10^{-12}	5.24×10^{-5}	1.63×10^{-12}	5.24×10^{-5}
	CD	2.94	1.96×10^{1}	1.97×10^{1}	6.05×10^{1}	6.12×10^{1}	8.57×10^{1}
	RCD	8.68	1.08×10^{1}	1.38×10^{1}	8.24×10^{1}	2.77×10^{1}	8.68×10^{1}
	Poly-3	8.52	4.06	9.42	8.73×10^{1}	1.25×10^{1}	8.82×10^{1}
	Poly-5	6.86×10^{-1}	4.47	4.48	2.62	1.67×10^{1}	1.67×10^{1}
	FIR	5.90	1.97	6.21	5.59×10^{1}	6.99	5.63×10^{1}

it recovers estimates with position errors in the km to tens of km, as well as velocity errors in the m/s to tens of m/s. These values are within the assumed initial standard deviations of sequential filters tested in the literature,[21,23,26] which indicates the relevance of this algorithm for initial state estimation. The performance strongly depends on the relative acceleration estimate, and we recommend utilizing more data, when possible, for a more robust result than with central differencing.

In future work, we would like to combine multiple estimates in a formation. We would also like to study efficient ways to eliminate the symmetric solution. Finally, we would like to explore the path to a solution without estimating the relative acceleration.

ACKNOWLEDGMENT

The authors thank the Georgia Tech Research Institute Independent Research and Development (IRAD) program for supporting this work.

Table 7: Values of $\boldsymbol{R}_{\boldsymbol{p}_1^j}$ in the LLO scenario with central difference, obtained with the analytical expression at Eq. (33) using a set of perfect measurements $\Delta\boldsymbol{r}_{12}$. Units of position are km and units of velocity are km/s.

6.99 $\times 10^{2}$	-1.56 $\times 10^{2}$	7.10 $\times 10^{2}$	5.42 $\times 10^{-1}$	-3.82 $\times 10^{-2}$	5.85 $\times 10^{-1}$
-1.56 $\times 10^{2}$	4.66 $\times 10^{1}$	-1.67 $\times 10^{2}$	-1.21 $\times 10^{-1}$	2.12 $\times 10^{-2}$	-1.36 $\times 10^{-1}$
7.10 $\times 10^{2}$	-1.67 $\times 10^{2}$	7.46 $\times 10^{2}$	5.50 $\times 10^{-1}$	-4.38 $\times 10^{-2}$	6.14 $\times 10^{-1}$
5.42 $\times 10^{-1}$	-1.21 $\times 10^{-1}$	5.50 $\times 10^{-1}$	5.35 $\times 10^{-4}$	-1.32 $\times 10^{-4}$	5.34 $\times 10^{-4}$
-3.82 $\times 10^{-2}$	2.12 $\times 10^{-2}$	-4.38 $\times 10^{-2}$	-1.32 $\times 10^{-4}$	1.23 $\times 10^{-4}$	-1.17 $\times 10^{-4}$
5.85 $\times 10^{-1}$	-1.36 $\times 10^{-1}$	6.14 $\times 10^{-1}$	5.34 $\times 10^{-4}$	-1.17 $\times 10^{-4}$	5.87 $\times 10^{-4}$

Table 8: Values of $\boldsymbol{R}_{\boldsymbol{p}_1^j}$ in the LLO scenario with central difference, obtained with a Monte-Carlo simulation of 100,000 samples. Units of position are km and units of velocity are km/s.

7.03 $\times 10^{2}$	-1.56 $\times 10^{2}$	7.14 $\times 10^{2}$	5.45 $\times 10^{-1}$	-3.71 $\times 10^{-2}$	5.87 $\times 10^{-1}$
-1.56 $\times 10^{2}$	4.70 $\times 10^{1}$	-1.68 $\times 10^{2}$	-1.22 $\times 10^{-1}$	2.14 $\times 10^{-2}$	-1.36 $\times 10^{-1}$
7.14 $\times 10^{2}$	-1.68 $\times 10^{2}$	7.51 $\times 10^{2}$	5.53 $\times 10^{-1}$	-4.29 $\times 10^{-2}$	6.17 $\times 10^{-1}$
5.45 $\times 10^{-1}$	-1.22 $\times 10^{-1}$	5.53 $\times 10^{-1}$	5.42 $\times 10^{-4}$	-1.34 $\times 10^{-4}$	5.37 $\times 10^{-4}$
-3.71 $\times 10^{-2}$	2.14 $\times 10^{-2}$	-4.29 $\times 10^{-2}$	-1.34 $\times 10^{-4}$	1.25 $\times 10^{-4}$	-1.16 $\times 10^{-4}$
5.87 $\times 10^{-1}$	-1.36 $\times 10^{-1}$	6.17 $\times 10^{-1}$	5.37 $\times 10^{-4}$	-1.16 $\times 10^{-4}$	5.88 $\times 10^{-4}$

REFERENCES

[1] J. Kepler, *Astronomia Nova*. 10.3931/e-rara-558.

[2] K. Ferguson, *Tycho and Kepler: the unlikely partnership that forever changed our understanding of the heavens*. Bloomsbury Publishing USA, 2002.

[3] P. R. Escobal, *Methods of orbit determination.* Wiley, New York, 1965.

[4] D. A. Vallado, *Fundamentals of astrodynamics and applications*, Vol. 12. Springer Science & Business Media, 2001.

[5] J. W. Gibbs, *On the determination of elliptic orbits from three complete observations*, Vol. 4. National Academy of Sciences, 1889.

[6] C. L. Hollenberg and J. A. Christian, "Geometric Solutions for Problems in Velocity-Based Orbit Determination," *Journal of the Astronautical Sciences*, Vol. 67, 2019, 10.1007/s40295-019-00170-7.

[7] S. Laplace, "Mémoire sur la Détermination des Orbites des Comètes," *Mémoires de Mathématique et de Physique*, 1780, pp. 13–72.

[8] C. F. Gauss and C. H. Davis, *Theory of the motion of the heavenly bodies moving about the sun in conic sections: a translation of Gauss's" Theoria Motus." with an appendix*. Little, Brown, 1857.

[9] R. H. Gooding, "A new procedure for the solution of the classical problem of minimal orbit determination from three lines of sight," *Celestial Mechanics and Dynamical Astronomy*, Vol. 66, 1997, 10.1007/BF00049379.

[10] J. A. Christian, "Initial Orbit Determination from Only Heading Measurements," *Journal of Spacecraft and Rockets*, 10.2514/1.A35593.

[11] E. S. Muller and P. M. Kachmar, "A New Approach to On-Board Orbit Navigation," *NAVIGATION*, Vol. 18, No. 4, 1971, 10.1002/j.2161-4296.1971.tb00109.x.

[12] P. K. Dave, *Autonomous navigation of distributed spacecraft using intersatellite laser communications*. PhD thesis, Massachusetts Institute of Technology, 2020.

[13] J. Kim and B. D. Tapley, "Simulation of Dual One-Way Ranging Measurements," *Journal of Spacecraft and Rockets*, Vol. 40, May 2003, 10.2514/2.3962.

[14] L. Gun and H. Feijiang, "Precise two way time synchronization for distributed satellite system," *2009 IEEE International Frequency Control Symposium Joint with the 22nd European Frequency and Time forum*, 2009, 10.1109/FREQ.2009.5168372.

[15] M. Alawieh, N. Hadaschik, N. Franke, and C. Mutschler, "Inter-satellite ranging in the Low Earth Orbit," *2016 10th International Symposium on Communication Systems, Networks and Digital Signal Processing (CSNDSP)*, 2016, 10.1109/CSNDSP.2016.7573920.

[16] L. M. Marrero, J. C. Merlano-Duncan, J. Querol, S. Kumar, J. Krivochiza, S. K. Sharma, S. Chatzinotas, A. Camps, and B. Ottersten, "Architectures and Synchronization Techniques for Distributed Satellite Systems: A Survey," *IEEE Access*, Vol. 10, 2022, 10.1109/ACCESS.2022.3169499.

[17] J. Griffin, A. Lindberg, T. Ahn, and P. Harton, "Shuttle rendezvous radar performance: evaluation and simulation," *IEEE Aerospace and Electronic Systems Magazine*, Vol. 4, No. 3, 1989, 10.1109/62.17933.

[18] K. Hill and G. H. Born, "Autonomous Interplanetary Orbit Determination Using Satellite-to-Satellite Tracking," *Journal of Guidance, Control, and Dynamics*, Vol. 30, No. 3, 2007, 10.2514/1.24574.

[19] F. Markley, "Autonomous navigation using landmark and intersatellite data," *AIAA/AAS Astrodynamics Conference*, 1984, 10.2514/6.1984-1987.

[20] M. L. Psiaki, "Autonomous Orbit Determination for Two Spacecraft from Relative Position Measurements," *Journal of Guidance, Control, and Dynamics*, Vol. 22, No. 2, 1999, 10.2514/2.4379.

[21] Y. Li and A. Zhang, "Observability analysis and autonomous navigation for two satellites with relative position measurements," *Acta Astronautica*, Vol. 163, 2019, 10.1016/j.actaastro.2019.02.030.

[22] M. L. Psiaki, "Absolute Orbit and Gravity Determination Using Relative Position Measurements Between Two Satellites," *Journal of Guidance, Control, and Dynamics*, Vol. 34, Sept. 2011, 10.2514/1.47560.

[23] P. Rocha Cachim, J. Gomes, and R. Ventura, "Autonomous orbit determination for satellite formations using relative sensing: Observability analysis and optimization," *Acta Astronautica*, Vol. 200, Nov. 2022, 10.1016/j.actaastro.2022.08.009.

[24] Y. Ou, H. Zhang, and B. Li, "Absolute orbit determination using line-of-sight vector measurements between formation flying spacecraft," *Astrophysics and Space Science*, Vol. 363, Mar. 2018, 10.1007/s10509-018-3293-2.

[25] O. Awad, I. Hwang, and M. Stoeckle, "A GPS-Free Navigation System for Earth-Orbiting Small Satellites," *44th Annual AAS Guidance, Navigation and Control (GN&C) Conference*, Breckenridge, CO, USA, February 2022.

[26] O. F. Awad, M. R. Stoeckle, and K. Oguri, "Gravity Model Error Compensation for Accurate Earth Orbit Determination of Two Satellites Using Relative Position Measurements Only," February 2023.

[27] J. Nocedal and S. J. Wright, *Numerical optimization*. Springer series in operations research, New York: Springer, 2nd ed ed., 10.1007/978-0-387-40065-5.

[28] B. Fornberg, "Generation of finite difference formulas on arbitrarily spaced grids," *Mathematics of computation*, Vol. 51, No. 184, 1988, 10.1090/S0025-5718-1988-0935077-0.

[29] T. Hastie, R. Tibshirani, and J. Friedman, *The Elements of Statistical Learning*. Springer Series in Statistics, New York, NY: Springer New York, 10.1007/978-0-387-84858-7.

[30] B. Kumar and S. Dutta Roy, "Design of digital differentiators for low frequencies," *Proceedings of the IEEE*, Vol. 76, No. 3, 1988, 10.1109/5.4408.

[31] P. Holoborodko, "Smooth Noise Robust Differentiators," `http://www.holoborodko.com/pavel/numerical-methods/numerical-derivative/smooth-low-noise-differentiators/`, 2008.

[32] "Design and Application of Digital FIR Differentiators Using Modulating Functions," Vol. 33, No. 15, 2000, 10.1016/S1474-6670(17)39890-7.

[33] S. Henry and J. A. Christian, "Absolute Triangulation Algorithms for Space Exploration," *Journal of Guidance, Control, and Dynamics*, Vol. 46, No. 1, 2023, 10.2514/1.G006989.

[34] F. L. Markley and J. L. Crassidis, *Fundamentals of spacecraft attitude determination and control*, Vol. 1286. Springer, 10.1007/978-1-4939-0802-8.

[35] P. W. Schumacher, C. Sabol, C. C. Higginson, and K. T. Alfriend, "Uncertain Lambert Problem," *Journal of Guidance, Control, and Dynamics*, Vol. 38, No. 9, 2015, 10.2514/1.G001019.

[36] R. R. Bate, D. D. Mueller, J. E. White, and W. W. Saylor, *Fundamentals of astrodynamics*. Dover Publications, 2020.